



# Electronic properties and superior CO<sub>2</sub> capture selectivity of metal nitride (XN) and phosphide (XP) (X = Al, Ga and In) sheets

Vivek K. Yadav<sup>a</sup>, Showkat H. Mir<sup>b</sup>, Jayant K. Singh<sup>a,\*</sup>

<sup>a</sup> Department of Chemical Engineering, IIT Kanpur, Kanpur 208016, India

<sup>b</sup> Department of Chemistry, IIT Kanpur, Kanpur 208016, India

## ARTICLE INFO

### Keywords:

Flue gas  
Adsorption energy  
Metal nitrides/phosphides  
Band gap  
Raman spectra

## ABSTRACT

In this work, we performed ab initio calculations to investigate the structural stability, carrier mobility, and CO<sub>2</sub> separation and capture ability of mono-layered group III nitrides (XN) and phosphides (XP) (X = Al, Ga, In). The results showed that all the six two-dimensional sheets exhibit indirect band gaps, ranging from 1.35 eV for InP to 4.02 eV for AlN by using HSE functional. Mobility calculations performed using deformation potential theory shows that the mobility is dominated by holes as compared to electrons and reaches a value of  $1.7 \times 10^3 \text{ cm}^2 \text{ V}^{-1} \text{ s}^{-1}$  for AlN and  $6.9 \times 10^2 \text{ cm}^2 \text{ V}^{-1} \text{ s}^{-1}$  AlP. Density functional perturbation theory was used to predict the frequency of Raman active modes, the results showed a red shift in the calculated Raman peak frequency with increase in the mass of metal ion. The calculated adsorption energy of CO<sub>2</sub> is in the range of  $-0.19 \text{ eV}$  to  $-0.22 \text{ eV}$  over XN, whereas the adsorption energy varies from  $-0.51 \text{ eV}$  to  $-1.12 \text{ eV}$  over XP, which is larger than that of graphene and hexagonal boron nitride. The adsorption energy of CO<sub>2</sub> on various nanostructures follows the order as  $E_{\text{InN}} > E_{\text{GaN}} > E_{\text{AlN}}$  and  $E_{\text{InP}} > E_{\text{GaP}} > E_{\text{AlP}}$ . On the other hand, it is seen that N<sub>2</sub> show significantly weaker interaction with the surfaces of XN and XP as compared to CO<sub>2</sub>, indicating high selectivity of sheets towards CO<sub>2</sub> capture.

## 1. Introduction

In response to the ever increasing calamity of global warming, the capture and storage of carbon dioxide (CO<sub>2</sub>) released by burning of fossil fuels will be an essential technology in the context of energy and environment [1]. Thus, identifying stable materials with improved capability for CO<sub>2</sub> capture has become an important target for capture and storage technologies [2,3]. Due to the increased emission rate of effluent gases (for instance, CO<sub>x</sub>, SO<sub>x</sub>, NO<sub>x</sub> etc.) from industries, gas adsorbent materials have engrossed a substantial attention from many researchers across the globe [4]. Among these greenhouse gases (GHGs), concentration of CO<sub>2</sub> in the atmosphere has increased rapidly (from 313 ppm in 1960 to 407 ppm in 2017), and is associated with the increased dependence on fossil fuels in the past century [5]. Therefore, reducing and capturing GHGs (e.g. CO<sub>2</sub>) from the atmosphere is a most challenging problem in environmental protection [6]. In recent years, processes such as adsorption, absorption, and use of membranes was used at large scale for capture and separation, however, these techniques pose a serious challenge in terms of efficiency [7]. In order to tackle the issue of global working, efficient capture of CO<sub>2</sub> and other GHGs through industrially proven and simple processes like adsorption

is of utmost importance. Although many gas adsorbent materials have been developed computationally and experimentally in the past, nevertheless, nanostructured materials possess potentially revolutionary advancements in the rapidly growing technological fields like environmental and sustainability engineering, energy storage and harvesting, and molecular sensing, etc [2,3,8,9]. This has led to a rapid increase in the development of gas adsorbent materials.

Among these nanostructured materials, 2D nanomaterials have received greater attention because of their unique properties that are attributed to their ultrathin thickness emerging due to quantum effects [5,10,11]. The 2D materials, which now can be synthesized either in single or multi-atomic layered forms have seen a huge interest from the past two decades [12–14]. Mono-layer materials not only exhibit a variety of new and useful optical, electronic and mechanical applications, but also show tremendous potential in the environmental application such as CO<sub>2</sub> capture and storage [15,16] as stated earlier.

In this work, we propose to investigate the group III metal nitrides and phosphides in the honeycomb crystal structure for CO<sub>2</sub> capture from flue gas using density functional theory (DFT). This paper is organized as follows: in Simulation methodology, we provide the details of the methods employed in the present work. In Results and discussion,

\* Corresponding author.

E-mail address: [jayantks@iitk.ac.in](mailto:jayantks@iitk.ac.in) (J.K. Singh).

<https://doi.org/10.1016/j.apsusc.2020.146445>

Received 7 October 2019; Received in revised form 4 March 2020; Accepted 3 April 2020

Available online 29 May 2020

0169-4332/ © 2020 Elsevier B.V. All rights reserved.

discuss the crystal structure and stability of XN and XP nanostructures and also through light on their Raman spectra. Then band structure and carrier mobility will be investigated. Subsequently, we present the adsorption energy of CO<sub>2</sub> and N<sub>2</sub> on XN and XP. We concluded the paper by giving a detailed summary of the main results of the present study with prospects of XN and XP nanostructures.

## 2. Simulation methodology

Density functional theory (DFT) calculations were performed to investigate the ground state properties of XN and XP (X = Al, Ga and In) mono-layers using QUANTUM ESPRESSO [17] code. The electron-ion interaction was described by Perdew-Burke-Ernzerhof [18] functional with generalized gradient approximation (GGA) [19]. To obtain optimized structure, the Kohn-Sham wave-functions were expanded by a plane wave basis set with a kinetic energy cutoff of 50 Ry for wave-function and 300 Ry for charge density. Brillouin zone (BZ) integration was done using a uniform  $\Gamma$ -centered Monkhorst-Pack [20] k-point grid of  $5 \times 5 \times 1$  for geometry optimization and  $15 \times 15 \times 1$  for self-consistent field calculations. The atomic positions and cell parameters were fully relaxed until an energy convergence of  $10^{-10}$  eV is achieved and force on each atom was smaller than  $0.03 \text{ eV}/\text{\AA}^{-1}$ . Van der Waals interactions were included using DFT-D3 dispersion corrections [21]. A vacuum of 20  $\text{\AA}$  was used in the z-direction to avoid any spurious interaction between periodic images. For calculation of gas phase atomic energies of CO<sub>2</sub> and N<sub>2</sub>, a simulation box was used with dimensions 15  $\text{\AA}$  to avoid interaction between periodic images. The energy of the molecular species in isolated form were calculated at the Gamma-point only. Also, to obtain a better description of the band gaps and more accurate positions of the CBM and VBM, we used HSE functional as implemented in QUANTUM ESPRESSO code, where the exchange part in the HSE functional consists of 25% from Hartree-Fock and 75% from GGA-PBE contributions. For calculations employing the HSE functional, we have used a k mesh of  $5 \times 5 \times 1$  to describe the Brillouin zone. The density functional perturbation theory (DFPT) was employed to calculate the phonon dispersion and Raman spectra in the linear response approach [22,23]. For phonon dispersion calculation, we used q-point grid of  $4 \times 4 \times 1$ . The standard norm-conserving local density functional (LDA) pseudopotentials [24] were used for Raman spectra calculations. The carrier mobility of various systems was also calculated in the deformation potential theory approximation using the relation [25–27],

$$\mu_{2D} = \frac{e\hbar^3 C^{2D}}{k_B T m^{*2} (E^i)^2} \quad (1)$$

where  $m^*$  represents the effective mass of charge carriers,  $E^i$  is the deformation potential constant of the conduction band minimum (CBM) for electrons or valence band maximum (VBM) for holes along the transport direction and is defined as,  $E^i = \Delta E_i/\varepsilon$ . Here  $\Delta E_i$  is the energy change of an  $i$ th band under the applied strain,  $\varepsilon$  represents the corresponding strain, which is defined as  $\varepsilon = \Delta a/a_0$ , where  $a_0$  is the equilibrium lattice constant in the transport direction and  $\Delta a$  is the deformation of  $a_0$ . The effective mass is calculated by the parabolic fitting of the E versus k curve ( $m^{*-1} = \frac{1}{\hbar^2} \frac{\partial^2 E}{\partial k^2}$ ) for holes and electrons in the vicinity of VBM and CBM, respectively. The elastic modulus  $C^{2D}$  along x- and y-direction is calculated as the second derivative of energy with respect to the applied strain per unit area as,  $C^{2D} = \frac{1}{A} \frac{d^2 E}{d\varepsilon^2}$ , where  $E$  denotes the total energy of the deformed system and  $A$  is the area of the system at equilibrium. The strain was varied from  $-2\%$  to  $2\%$  in steps of 0.5. All these parameters were calculated using PBE functional. The temperature used for mobility calculation was 300 K.

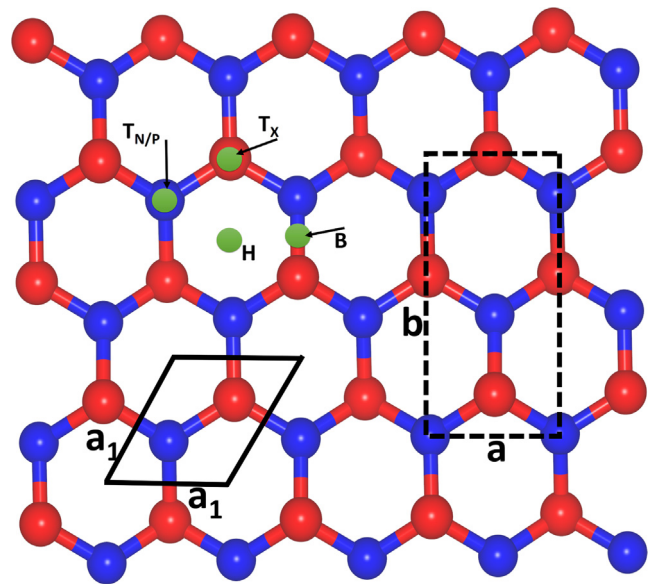


**Fig. 1.** Atomic structure model of mono-layer XN and XP (X = Al, Ga, and In) sheets. The dashed lines represent the rectangular cell used for mobility calculation have lattice constants  $a$  and  $b$ . The hexagonal unit cell with lattice constant  $a_1$  is shown by solid lines. Four adsorption sites are shown by green circles. (For interpretation of the references to colour in this figure legend, the reader is referred to the web version of this article.)

## 3. Results and discussions

### 3.1. Crystal structure and stability

The representative crystal structure of metal nitrides (XN) and phosphides (XP) (X = Al, Ga, and In) is presented in Fig. 1, in which hexagonal unit cell is marked by solid lines and lattice parameter by  $a_1$ . For calculating the carrier mobility using deformation potential theory, we constructed a rectangular super-cell which fulfills an intuitive presentation of carrier conduction along the zigzag ( $a$ ) and armchair ( $b$ ) directions. The calculated lattice parameters of the various 2D materials for the hexagonal unit cell are listed in Table 1. It is seen that both for nitrides and phosphides, the lattice parameter increases as the size of metal ion increase with GaP as an exception whose lattice parameter was found smaller than AlP. The results are consistent with the previous theoretical reports with  $a = 3.13\text{\AA}$ ,  $3.21\text{\AA}$ , and  $3.61\text{\AA}$  for AlN [28], GaN [29] and InN [30], respectively. For AlP, the calculated value of lattice parameter is also consistent with the theoretical results (3.92 eV) of Liu et al. [31]. Experimentally, Chen et al. has measured the lattice parameter of GaN in the range of 2.9–3.32  $\text{\AA}$  [32]. It can be inferred from these results that the structures and computational method we offered are reliable and accurate. Also, stability is an important factor of 2D materials for practical applications. The thermodynamic stability of XN and XP mono-layers were examined by calculating cohesive energy ( $E_{coh}$ ) using the equation  $E_{coh} = [E_{tot} - n_i E_X]/n$  ( $i = 1, 2$ ), where  $E_{tot}$  denotes the total energy of a system,  $E_X$  represents the gas phase atomic

**Table 1**

Lattice parameters ( $\text{\AA}$ ), band gap values (eV) and cohesive energy per atom (eV) of metal nitrides and phosphides.

System	$a_1$ ( $\text{\AA}$ )	$d_{X-N/P}$ ( $\text{\AA}$ )	PBE ( $E_{gap}$ )	HSE ( $E_{gap}$ )	$E_{coh}/atom$
AlN	3.13	1.80	2.91	4.02	-4.83
GaN	3.23	1.86	2.07	3.82	-3.77
InN	3.58	2.06	0.59	1.57	-2.65
AlP	3.93	2.27	2.33	3.22	-1.50
GaP	3.89	2.26	1.21	1.93	-1.15
InP	4.25	2.45	0.38	1.35	-0.42

energy of various elements and  $n_i$  is the total number of atoms in the sheet. The calculated cohesive energy calculated at PBE level of theory are shown in Table 1. Cohesive energy per atom calculated was  $-4.83$  eV,  $-3.77$  eV and  $-2.65$  eV for AlN, GaN and InN. One can see that cohesive energy decreases as the size of metal ion increase, which is consistent with the order of lattice parameter of the corresponding system. Other theoretical results also show similar behavior in cohesive energy for AlN ( $-5.36$  eV) and GaN ( $-4.04$  eV) [28,29]. The discrepancy in the calculated and literature values may be attributed to pseudopotentials and smearing method used. In our calculations, we have employed PBE functional with fermi-dirac smearing technique while the literature work was performed using Projected Augmented Wave method with gaussian smearing. For metal phosphides (AlP, GaP and InP) a similar trend in the cohesive energy was seen as displayed by metal nitrides, however, we did not find any theoretical or experimental literature on XP (except lattice parameter of AlP) to compare our results with. From cohesive energy results, it is apparent that metal nitrides are comparatively more stable than metal phosphides, which indicates that the former has strong bonded network compared to the latter. Moreover, the phonon dispersion of metal nitrides and phosphides were also calculated to explore their lattice dynamic stability as shown in Fig. 2. It is well known fact that phonon dispersion showing any soft mode (negative frequency) indicates the instability of a lattice [33]. From phonon dispersion, it is apparent that no soft modes are shown by the mono-layer metal nitrides, thus representing their dynamic stability. On the other hand, it is observed that metal phosphides contain soft phonon branches in the phonon dispersion, which indicates instability of their lattices. The highest phonon frequency of XN ( $A = \text{Al, Ga and In}$ ) mono-layers are about  $1000$ ,  $838$ , and  $700$   $\text{cm}^{-1}$ , which are much higher than the highest frequency of  $580$   $\text{cm}^{-1}$  in silicene [34],  $473$   $\text{cm}^{-1}$  in  $\text{MoS}_2$  [35] mono-layer, indicating robust X-N bonds in XN mono-layers.

The Raman spectra of mono-layer metal nitrides was also simulated as shown in Fig. 3 (we did not simulate Raman spectra of metal phosphides as their phonon dispersion contained softmodes). In the Raman spectra, there exists one peak ( $E_g$  modes) in each of the structures, which are all doubly degenerate in-plane modes. Raman spectra provide evidence to identify synthesized 2D materials in experiments. The Raman peak frequencies calculated for AlN, GaN, and InN were  $815$   $\text{cm}^{-1}$ ,  $740$   $\text{cm}^{-1}$ , and  $685$   $\text{cm}^{-1}$ , respectively. The peak

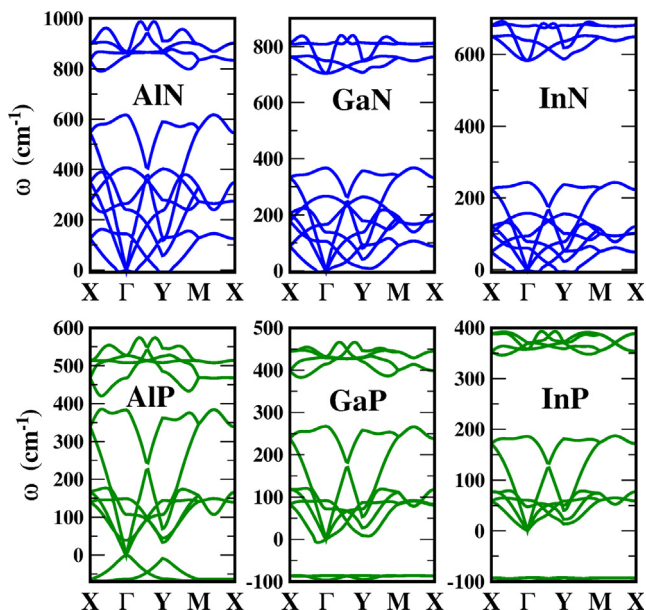


Fig. 2. Phonon band structure of AlN, GaN, InN, AlP, GaP, and InP exhibiting their lattice dynamic stability.

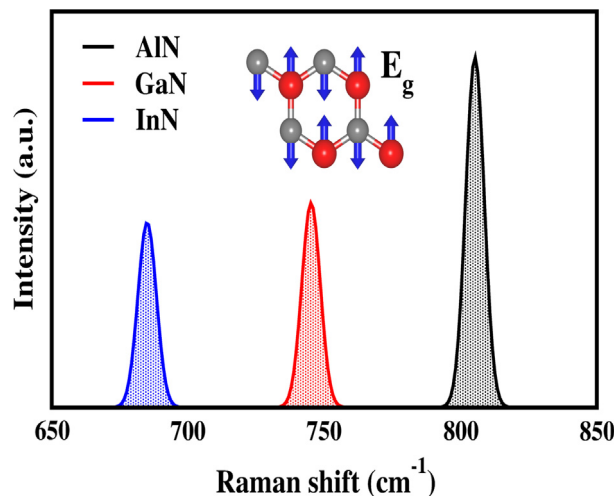


Fig. 3. The calculated Raman active modes of metal nitrides. A convolution of the computed DFT spectra with Gaussian profile and  $5$   $\text{cm}^{-1}$  line-width was performed for better visualization using Magicplot software [36]. The inset shows the corresponding representative vibrational mode. In the inset, Red and gray balls indicate metal and nitrogen atom, respectively.

frequencies were fitted by Gaussian profile with  $5$   $\text{cm}^{-1}$  line width using Magicplot software [36]. A red shift is seen in the peak frequency from AlN to InN, which is attributed to the mass of the metal ions, i.e. as mass increases, the frequency decreases.

### 3.2. Electronic band structure and mobility

Fig. 4 shows the band structures of mono-layer XN and XP at PBE level. All the structures are semiconductors and were found to show indirect band gaps. The conduction band minimum (CBM) is situated at the  $\Gamma$ -point and valence band maximum (VBM) occurs along the  $\Gamma$ -X direction of the irreducible Brillouin zone. As expected the VBM is mainly attributed to the p orbital of pnictogen atom (N/P) while the CBM is associated mainly with p orbital of X ( $X = \text{Al, Ga, and In}$ ) as shown in Figs. S1 and S2. The calculated band gaps at PBE level were  $2.91$  eV,  $2.07$  eV and  $0.59$  eV for AlN, GaN and GaP whereas the band gaps calculated for AlP, GaP and InP are  $2.33$  eV,  $1.21$  eV and  $0.38$  eV, respectively. Theoretical band gaps predicted for AlN and GaN mono-layers were  $2.9$  eV [28] and  $2.16$  eV [29] at PBE level are consistent with our results calculated at the same level of theory. It is found that

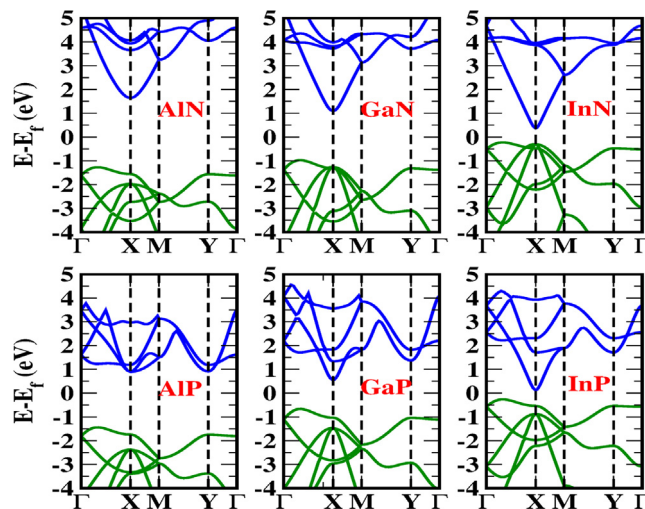


Fig. 4. The electronic band dispersion of metal nitrides and phosphides calculated at PBE level. The Fermi energy is set at  $0$  eV.

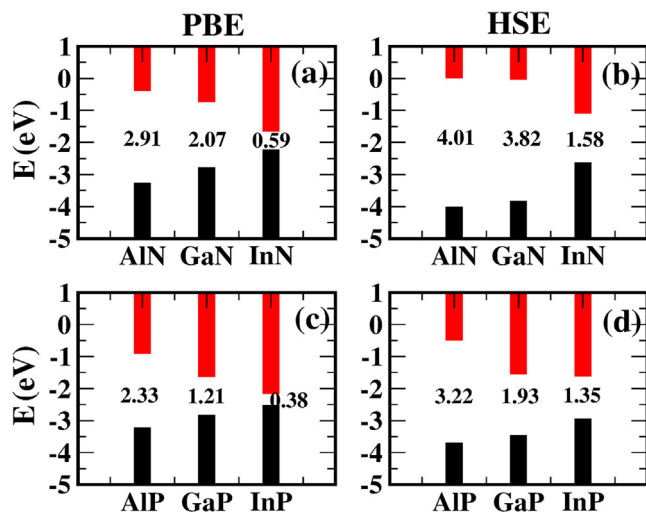


Fig. 5. The bandgap values of metal nitrides and phosphides calculated using (a,c) PBE and (b,d) HSE functionals.

metal phosphides show comparatively smaller band gaps than the metal nitrides. As DFT-PBE often underestimates the band gaps, we also calculated the band gaps at the HSE level for comparison (Fig. 5). From HSE calculations, it is seen that AlN, GaN and AlP show more than 3 eV band gaps. In fact, AlN were found to show band gap of 4.01 eV which renders it an insulating material. On the other hand, InN, GaP and InP were found to show less than 2 eV band gap, which makes them highly attractive for electronic applications. The calculated band gap of InN (AlP) was 1.57 eV (3.22 eV), these values are consistent with the theoretical results with values 1.52 eV (3.24 eV) calculated by Zhuang et al. at the HSE level [15]. The band gap value calculated for GaN by Peng et al. were 3.177 eV and 3.687 eV using HSE03 and HSE06 functionals, respectively and matches well to our result of 3.82 eV calculated at HSE functional [37]. Despite different band gap values of metal nitrides and phosphides, we observe that these materials exhibit almost the same band shapes near the Fermi level, i.e., a similar parabolic shape.

To further investigate the potential 2D metal nitrides and phosphides for device applications, we calculated the electron and hole mobility. The mobility of carriers and other related parameters such as effective mass, deformation potential and elastic constants are given in Table 2. Effective masses of electron and hole along x- and y-direction were calculated at CBM and VBM, respectively. It can be noticed from the Table 2 that the effective mass of hole is more than two times larger

Table 2

Carrier, 'e' and 'h' denote electron and hole, respectively and  $m^*$  is the effective mass of carriers.  $\lambda_x$ ,  $\lambda_y$ ,  $C_x^{2D}$  and  $C_y^{2D}$  represents the scattering probability and elastic constants along x- and y-direction,  $\mu_x$  and  $\mu_y$  denote the mobility in  $\text{cm}^2 \text{V}^{-1} \text{s}^{-1}$ .

System	Carrier	$m^*/m_0$	$\lambda_x$	$\lambda_y$	$C_x^{2D}$	$C_y^{2D}$	$\mu_x$	$\mu_y$
AlN	e	1.6	8.35	8.39	114.1	113.52	105.6	105.1
	h	2.9	0.15	0.23	114.1	113.52	1734.5	1104.5
GaN	e	0.9	38.69	38.81	108.6	108.3	72.1	71.9
	h	2.3	1.91	1.92	108.6	108.3	223.8	223.2
InN	e	0.8	30.63	29.6	63.9	63.1	115.4	119.4
	h	2.8	2.38	2.03	63.9	63.1	120.9	142.1
AlP	e	1.0	103.59	103.94	57.5	57.3	21.8	21.7
	h	1.9	0.90	1.18	57.5	57.3	694.5	529.8
GaP	e	0.4	147.48	143.86	62.1	62.3	95.8	98.3
	h	1.4	3.34	3.33	62.1	62.3	345.3	346.5
InP	e	0.6	99.02	102.61	43.8	43.6	63.5	61.2
	h	1.5	2.92	2.94	43.8	43.6	343.4	342.2

$m_0$  is the rest mass of electron.

compared to the electron mass. From this one may infer that electron should have higher mobility than hole as mobility is inversely proportional to the effective mass. However, it can be noted from the Table 2 that hole mobility dominates over electron mobility. This behavior can be explained on the basis of parameter  $\lambda$ , which measures the scattering of carriers with phonons (in present work, we primarily focused on the acoustic phonon-limited mobility, which dominates for small bias voltages). As can be seen from the table that  $\lambda$  is significantly larger for electrons than holes and thus limits the mobility of electrons. Furthermore, the elastic constants carrier mobility are found to be comparable along x- and y-directions, which is due to the fact that all materials exhibit hexagonal symmetry and have similar environment for atoms along the two directions. The small differences may be due to numerical errors. For metal nitrides, it is found that hole mobility dominates over the electron mobility. A similar trend was seen for metal phosphides also.

### 3.3. Adsorption energy of $\text{CO}_2$ and $\text{N}_2$

Efficient separation and capture of  $\text{CO}_2$  from gas mixtures such as from post-combustion gases (with mainly  $\text{N}_2/\text{CO}_2$  mixtures) has been a challenging task to the reduction of atmospheric  $\text{CO}_2$  accumulation, thereby global warming. To this goal, developing cost-effective and robust sorption materials is important. To find the most favorable adsorption configuration of  $\text{CO}_2$  as well as  $\text{N}_2$  on XN and XP (X = Al, Ga and In), several typical adsorption sites, including the top site over nitrogen/phosphorus ( $T_{N/P}$ ), bridge site (B) over metal-nitrogen/phosphorus bond, hollow site (H) above the center of hexagonal ring and top site ( $T_X$ ) over metal atom of the sheet were examined for adsorption of gas molecules. Two orientations were considered for adsorption of  $\text{CO}_2$  and  $\text{N}_2$  (i) the bond axis of the molecules is perpendicular (ver) and (ii) parallel (par) to the adsorbent surface. The adsorption energy of  $\text{CO}_2$  ( $\text{N}_2$ ) on to the XN and XP (X = Al, Ga and In) surface is computed as

$$E_{\text{ads}} = E_{\text{system}+\text{Y}} - (E_{\text{system}} + E_{\text{Y}}) \quad (2)$$

where  $E_{\text{system}+\text{Y}}$  is the total energy of the system after adsorption of gas molecules,  $E_{\text{system}}$  is the energy of pure metal nitride sheet without adsorbed species, and  $E_{\text{Y}}$  is the total energy of the isolated molecule. BY the definition of Eq. (2), the more negative value of  $E_{\text{ads}}$  corresponds to the most favorable adsorption configuration. To calculate the adsorption energy we adopted a supercell containing 48 atoms. The optimised lattice parameters of 48 atom unit cell are given in Table S1. A full summary of adsorption energies of  $\text{CO}_2$  and  $\text{N}_2$  at the above mentioned sites in both orientations are listed in Table S2 and S3, respectively. The most favorable adsorption site of  $\text{CO}_2$  molecule over XN and XP was found  $T_X$  as shown in Table 3. In all cases, it was found that parallel configuration is energetically favorable for  $\text{CO}_2$  than perpendicular orientation. On the contrary, it is seen that both parallel and perpendicular orientation as well as mixed adsorption sites are possible for  $\text{N}_2$  depending on the adsorbent surface. The calculations show that perpendicular orientation is energetically favorable for  $\text{N}_2$  on all 2D materials except over InN sheet. It was found that on AlN, GaN and InP  $\text{N}_2$  binds over the B-site while  $T_X$  site is most stable site over AlP and GaP.  $T_X$  site with parallel orientation was found stable over InN. Figs. S3 and S4 show the optimized structures of  $\text{CO}_2$  and  $\text{N}_2$  molecules on various sheets at the most stable adsorption sites. The binding strength of  $\text{CO}_2$  on metal nitrides follows the order as  $E_{\text{InN}} > E_{\text{GaN}} > E_{\text{AlN}}$  where as on metal phosphides the observed order was  $E_{\text{InP}} > E_{\text{GaP}} > E_{\text{AlP}}$ . It is found that adsorption energy of  $\text{CO}_2$  on AlP, GaP and InP is approximately two and a half, three and five times than that of metal nitrides. Also, It is apparent from Table 3 that adsorption energy of  $\text{CO}_2$  on metal nitride nanostructures is significantly larger than that of  $\text{MoS}_2$  ( $-0.13$  eV) [5] and graphene ( $-0.15$  eV) [5]. The adsorption energy of  $\text{CO}_2$  on h-BN sheet is  $-0.44$  eV which is comparable to AlP and GaP. The highest adsorption energy of  $\text{CO}_2$  was calculated on InP ( $-1.06$  eV), which arises due to substantial bending of InP due to adsorbent. Nevertheless,

**Table 3**

Adsorption energy of CO<sub>2</sub> and N<sub>2</sub> on XN and XP (X = Al, Ga and In) sheets, d is the equilibrium distance of C and N atoms in molecules from the nearest metal atom off the sheet and b denotes the C–O and N–N equilibrium bond lengths of CO<sub>2</sub> and N<sub>2</sub> molecules on 2D sheets. Superscripts “h” and “v” on the adsorption site indicates the horizontal and vertical configuration of molecules, respectively. The adsorption energy was calculated using PBE functional.

System	CO <sub>2</sub>				N <sub>2</sub>			
	E <sub>ads</sub> (eV)	d(Å)	b(Å)	Ads. site	E <sub>ads</sub> (eV)	d(Å)	b(Å)	Ads. site
AlN	−0.19	3.20	1.17	T <sub>N</sub> <sup>h</sup>	−0.09	2.98	1.11	B <sup>v</sup>
GaN	−0.20	3.47	1.17	T <sub>N</sub> <sup>h</sup>	−0.08	3.30	1.11	B <sup>v</sup>
InN	−0.22	3.14	1.17	T <sub>N</sub> <sup>h</sup>	−0.05	4.55	1.11	T <sup>h</sup>
AlP	−0.51	3.63	1.17	T <sub>P</sub> <sup>h</sup>	−0.23	2.19	1.11	T <sup>v</sup>
GaP	−0.59	3.45	1.17	T <sub>P</sub> <sup>h</sup>	−0.07	3.39	1.11	T <sup>v</sup>
InP	−1.12	3.72	1.17	T <sub>P</sub> <sup>h</sup>	−0.96	3.88	1.11	B <sup>v</sup>
h-BN <sup>a</sup>	−0.44				−0.24			

<sup>b</sup>Theoretical adsorption energy of CO<sub>2</sub> on mono-layer MoS<sub>2</sub> and graphene is −0.13 eV and −0.15 eV, respectively calculated using DFT-D2.

a = Ref [16], b = Ref[5]

our results are more interesting and useful as they show more selectivity towards CO<sub>2</sub> than N<sub>2</sub>.

Also, for adsorption energy calculations, initially, the CO<sub>2</sub> molecule was positioned at a distance of 3 Å from the adsorbent, after optimization, the equilibrium distance between adsorbate and adsorbent found were less than the initial distances as shown in Table 3, which is an indication of physisorption of CO<sub>2</sub> molecules. The significant binding of CO<sub>2</sub> to metal nitrides and phosphides nanostructures suggests a possible avenue for carbon dioxide capture applications. With this in mind, it was important to check the relative strength of adsorption of other small gas molecules on the surfaces of mono-layer nanostructures. Nitrogen is selected as the most relevant point of comparison because it is abundant in the atmosphere and also in the factory flue gas. The adsorption energies of N<sub>2</sub> are much weaker than that of CO<sub>2</sub>, which indicates that N<sub>2</sub> experiences only a weak interaction with the metal nitrides and phosphides nanostructures. Thus, our calculations indicate the application potential of group-III nitride and phosphide based materials in carbon dioxide capture and storage. In view of the fact that carbon dioxide exhibit optimum binding strength with AN and AP nanostructures at ambient temperature, whereas nitrogen does not, it may be concluded that both AN and AP sheets display considerable selectivity for adsorption of CO<sub>2</sub> from air or exhaust flue gases. Here, we should also note that the interaction of XN and XP with other contaminants, such as H<sub>2</sub>O, HCl, NH<sub>3</sub>, H<sub>2</sub>S, etc., is also very interesting and such calculations are intended for future work.

To analyse the effect of CO<sub>2</sub> and N<sub>2</sub> on the electronic properties of mono-layer sheets, the projected density of states (PDOS) of pristine sheets as well as CO<sub>2</sub>/N<sub>2</sub> doped sheets were computed (Figs. S2 and S3). In the case of pristine systems, it is seen that valence band is comprised of N (P) p-orbitals for XN (XP) sheets while the conduction band is a mixture of metal and N(P) p-orbitals with a major contribution from non-metal elements (N or P). Also from PDOS, it is apparent that CO<sub>2</sub>/N<sub>2</sub> adsorption modulates the electronic band structure of sheets in different manners: for XN, it is seen that N<sub>2</sub> introduces an energy level in the band gap near the conduction band, therefore its adsorption will decrease the band gap. While C and O orbitals in CO<sub>2</sub> introduces an energy state near the conduction band in AlN, however, these orbitals overlap with the conduction band of GaN and InN. On the other hand, in metal phosphides, the N p-orbitals overlap with the conduction band of XP sheets whereas CO<sub>2</sub> does not introduce an energy state in the band gap or conduction band but there are few O-states deep in the valence band.

## 4. Conclusions

DFT calculations were performed to investigate the structural stability and electron/phonon properties of planar metal nitrides and phosphides besides CO<sub>2</sub> adsorption. Calculated cohesive energy per atom indicated that XN are energetically more stable than XP. For XN mono-layers, it was found that cohesive energy per atom is maximum for AlN (−4.83 eV) and minimum for InN (−2.65 eV) and follows the order as AlN>GaN>InN, i.e. cohesive energy per atom decreases as the size of metal ion increases. A similar trend in the cohesive energy was seen for XP. Also, from phonon dispersion, it was revealed that mono-layer XN are dynamically stable whereas softmodes were seen in the phonon dispersion of XP which indicates their dynamical instability. The calculated band gaps of 2.91 eV (2.33 eV), 2.07 eV (1.21 eV) and 0.59 eV (0.38 eV) were found for AlN (AlP), GaN (GaP) and InN (InP), respectively at PBE level of theory. Likewise cohesive energy, the bandgap of both XN and XP were found to decrease as the size of metal ion increases. The carrier mobility was found maximum for AlN (1734.5 cm<sup>2</sup> V<sup>−1</sup> s<sup>−1</sup>) and minimum for InP (61.2 cm<sup>2</sup> V<sup>−1</sup> s<sup>−1</sup>) and was found to be dominant by holes for all nanostructures. The adsorption energy calculations showed that CO<sub>2</sub> binds strongly to metal phosphides as compared to the metal nitrides. The adsorption energy of CO<sub>2</sub> was −0.51 eV, −0.59 eV and −1.12 eV for AlP, GaP and InP, respectively, while it was about −0.20 eV for metal nitrides. It was found that CO<sub>2</sub> adsorbs over N/P atom in the horizontal orientation on all 2D sheets. These results were found to be superior than MoS<sub>2</sub> (−0.13 eV) and graphene(−0.15 eV). The adsorption energy of N<sub>2</sub> of different adsorbents was substantially smaller than that of CO<sub>2</sub>, which demonstrate the high selectivity of XN and XP towards CO<sub>2</sub> adsorption from flue gas. It is thus concluded that metal nitrides/phosphides are potential candidate materials for adsorption of CO<sub>2</sub> from flue gas and need to be experimentally verified.

## CRedit authorship contribution statement

**Vivek K. Yadav:** System setup, analyzing data and Writing - original draft. **Showkat H. Mir:** Analyzing data and Writing - original draft. **Jayant K. Singh:** Supervision.

## Declaration of Competing Interest

The authors declare that they have no known competing financial interests or personal relationships that could have appeared to influence the work reported in this paper.

## Acknowledgment

VKY gratefully acknowledge the financial support from Department of Science and Technology (Grant No. SB/S3/CE/079/2015 and DST/TM/WTI/2K15/112(G)). SHM thank Department of Chemistry, IIT Kanpur for IPDF. We also sincerely acknowledge High Performance Computing Facility of Computer Center at IIT Kanpur.

## Appendix A. Supplementary material

Supplementary data associated with this article can be found, in the online version, at <https://doi.org/10.1016/j.apsusc.2020.146445>.

## References

- [1] Yan Jiao, Du. Aijun, Zhonghua Zhu, Victor Rudolph, Sean C. Smith, Adsorption of carbon dioxide and nitrogen on single-layer aluminum nitride nanostructures studied by density functional theory, *J. Phys. Chem. C* 114 (17) (2010) 7846–7849.
- [2] J. Li, M. Hou, Y. Chen, W. Cen, Y. Chu, S. Yin, Enhanced CO<sub>2</sub> capture on graphene via N, S dual-doping, *Appl. Surf. Sci.* 399 (2017) 420–425.
- [3] Sherif Abdulkader Tawfik, X.Y. Cui, S.P. Ringer, C. Stampfl, Multiple CO<sub>2</sub> capture in stable metal-doped graphene: a theoretical trend study. *RSC, Advances* 5 (63)

- (2015) 50975–50982.
- [4] Claudio Cazorla, The role of density functional theory methods in the prediction of nanostructured gas-adsorbent materials, *Coord. Chem. Rev.* 300 (2015) 142–163.
- [5] Francis M. Enejekwu, Collins I. Ezech, Michael W. George, Xu. Mengxia, Hainam Do, Yue Zhang, Haitao Zhao, Wu. Tao, A comparative study of mechanisms of the adsorption of CO<sub>2</sub> confined within graphene-MoS<sub>2</sub> nanosheets: a DFT trend study, *Nanoscale Adv.* 1 (4) (2019) 1442–1451.
- [6] R.F. Service, The carbon conundrum, *Science (New York, NY)* 305(5686) (2004) 962.
- [7] Anand B. Rao, Edward S. Rubin, A technical, economic, and environmental assessment of amine-based CO<sub>2</sub> capture technology for power plant greenhouse gas control, *Environ. Sci. Technol.* 36 (20) (2002) 4467–4475.
- [8] L. Ci, L. Song, C. Jin, D. Jariwala, D. Wu, Y. Li, A. Srivastava, Z.F. Wang, K. Storr, L. Balicas, F. Liu, Atomic layers of hybridized boron nitride and graphene domains, *Nature Mater.* 9 (5) (2002) 430.
- [9] Dong Wang, Panyue Wen, Jian Wang, Lei Song, Hu. Yuan, The effect of defect-rich molybdenum disulfide nanosheets with phosphorus, nitrogen and silicon elements on mechanical, thermal, and fire behaviors of unsaturated polyester composites, *Chem. Eng. J.* 313 (2017) 238–249.
- [10] C. Lee, Q. Li, W. Kalb, X.Z. Liu, H. Berger, R.W. Carpick, J. Hone, Frictional characteristics of atomically thin sheets, *Science* 328 (5974) (2010) 76–80.
- [11] Kostya S. Novoselov, D. Jiang, F. Schedin, T.J. Booth, V.V. Khotkevich, S.V. Morozov, Andre K. Geim, Two-dimensional atomic crystals, *Proc. Natl. Acad. Sci.* 102 (30) (2005) 10451–10453.
- [12] Peter W. Sutter, Jan-Ingo Flege, Eli A. Sutter, Epitaxial graphene on ruthenium, *Nature Mater.* 7 (5) (2008) 406.
- [13] Colin L. Freeman, Frederik Claeyssens, Neil L. Allan, John H. Harding, Graphitic nanofilms as precursors to wurtzite films: theory, *Phys. Rev. Lett.* 96 (6) (2006) 066102.
- [14] Dangxin Wu, M.G. Lagally, Feng Liu, Stabilizing graphitic thin films of wurtzite materials by epitaxial strain, *Phys. Rev. Lett.* 107 (23) (2011) 236101.
- [15] Houlong L. Zhuang, Arunima K. Singh, Richard G. Hennig, Computational discovery of single-layer III-V materials, *Phys. Rev. B* 87 (16) (2013) 165415.
- [16] Hongyan Guo, Wenhua Zhang, Ning Lu, Zhiwen Zhuo, Xiao Cheng Zeng, Xiaojun Wu, Jinlong Yang, CO<sub>2</sub> capture on h-BN sheet with high selectivity controlled by external electric field, *J. Phys. Chem. C* 119 (12) (2015) 6912–6917.
- [17] P. Giannozzi, S. Baroni, N. Bonini, M. Calandra, R. Car, C. Cavazzoni, D. Ceresoli, G.L. Chiarotti, M. Cococcioni, I. Dabo, et al., QUANTUM ESPRESSO: a modular and open-source software project for quantum simulations of materials, *J. Phys.: Condens. Matter* 21 (39) (2009) 395502.
- [18] J.P. Perdew, K. Burke, M. Ernzerhof, Generalized gradient approximation made simple, *Phys. Rev. Lett.* 77 (18) (1996) 3865.
- [19] J.P. Perdew, J.A. Chevary, S.H. Vosko, K.A. Jackson, M.R. Pederson, D.J. Singh, C. Fiolhais, Atoms, molecules, solids, and surfaces: Applications of the generalized gradient approximation for exchange and correlation, *Phys. Rev. B* 46 (1992) 6671.
- [20] H.J. Monkhorst, J.P. Pack, Special points for Brillouin-zone integrations, *Phys. Rev. B* 13 (1976) 5188.
- [21] S. Grimme, J. Antony, S. Ehrlich, H. Krieg, A consistent and accurate ab initio parametrization of density functional dispersion correction (DFT-D) for the 94 elements H-Pu, *J. Chem. Phys.* 132 (2010) 154104.
- [22] Stefano Baroni, Stefano De Gironcoli, Andrea Dal Corso, Paolo Giannozzi, Phonons and related crystal properties from density-functional perturbation theory, *Rev. Mod. Phys.* 73 (2) (2001) 515.
- [23] S.H. Mir, P.C. Jha, S. Dabhi, P.K. Jha, ab initio study of phase stability, lattice dynamics and thermodynamic properties of magnesium chalcogenides, *Mater. Chem. Phys.* 175 (2016) 54–61.
- [24] D.R. Hamann, M. Schlüter, C. Chiang, Norm-conserving pseudopotentials, *Phys. Rev. Lett.* 43 (20) (1979) 1494.
- [25] V.K. Yadav, S.H. Mir, J.K. Singh, A computational study of structural, electronic and carrier mobility of boron and phosphorus/nitrogen co-doped graphene, *Physica B* 571 (2019) 291–295.
- [26] S.H. Mir, Exploring the electronic, charge transport and lattice dynamic properties of two-dimensional phosphorene, *Physica B* 572 (2019) 88–93.
- [27] S. Bruzzone, G. Fiori, Ab-initio simulations of deformation potentials and electron mobility in chemically modified graphene and two-dimensional hexagonal boron-nitride, *Appl. Phys. Lett.* 99 (2011) 222108.
- [28] C. Bacaksiz, H. Sahin, H.D. Ozaydin, S. Horzum, Ramazan Tug̃rul Senger, François M. Peeters, Hexagonal AlN: Dimensional-crossover-driven band-gap transition, *Phys. Rev. B* 91 (8) (2015) 085430.
- [29] A. Onen, D. Kecik, E. Durgun, S. Ciraci, GaN: From three-to two-dimensional single-layer crystal and its multilayer van der Waals solids, *Phys. Rev. B* 93 (8) (2016) 085431.
- [30] M.S. Prete, O. Pulci, F. Bechstedt, Strong in-and out-of-plane excitons in two-dimensional InN nanosheets, *Phys. Rev. B* 98 (2018) 235431.
- [31] C.S. Liu, Z.W. Teng, X.J. Ye, X.H. Yan, Two-dimensional tetragonal AIP monolayer: strain-tunable direct–indirect band-gap and semiconductor-metal transitions, *J. Mater. Chem. C* 5 (2017) 5999–6004.
- [32] Y. Chen, K. Liu, J. Liu, T. Lv, B. Wei, T. Zhang, M. Zeng, Z. Wang, L. Fu, Growth of 2D GaN single crystals on liquid metals, *J. Am. Chem. Soc.* 140 (2018) 16392–16395.
- [33] Showkat H. Mir, Prakash C. Jha, Muhammed Shafiqul Islam, Amitava Banerjee, Wei Luo, Shweta D. Dabhi, Prafulla K. Jha, Rajeev Ahuja, Static and dynamical properties of heavy actinide mononitrides of lutetium, *Sci. Rep.* 6 (2016) 29309.
- [34] Seymur Cahangirov, Mehmet Topsakal, Ethem Aktürk, H. Ažahin, Salim Ciraci, Two-and one-dimensional honeycomb structures of silicon and germanium, *Phys. Rev. Lett.* 102 (23) (2009) 236804.
- [35] Alejandro Molina-Sanchez, Ludger Wirtz, Phonons in single-layer and few-layer MoS<sub>2</sub> and WS<sub>2</sub>, *Phys. Rev. B* 84 (15) (2011) 155413.
- [36] <https://magicplot.com/>.
- [37] B. Peng, H. Zhang, H. Shao, K. Xu, G. Ni, L. Wu, J. Li, H. Lu, Q. Jin, H. Zhu, Room-temperature bound exciton with long lifetime in monolayer GaN, *ACS Photonics* 5 (2018) 4081–4088.